SIAM J. SCI. COMPUT.
Vol. 33, No. 3, pp. 1395–1414

AN ADAPTIVE TIME-STEPPING STRATEGY FOR THE MOLECULAR BEAM EPITAXY MODELS*

ZHONGHUA QIAO†, ZHENGRU ZHANG‡, AND TAO TANG†

Abstract. This paper is concerned with the numerical simulations for the dynamics of the molecular beam epitaxy (MBE) model. The numerical simulations of the MBE models require long time computations, and therefore large time-stepping methods become necessary. In this work, we consider some unconditionally energy stable finite difference schemes, which will be used in the time adaptivity strategies. It is found that the use of the time adaptivity cannot only resolve the steady-state solutions but also the dynamical changes of the solution accurately and efficiently. The adaptive time step is selected based on the energy variation or the change of the roughness of the solution. The numerical experiments demonstrated that the CPU time is significantly saved for long time simulations.

Key words. molecular beam epitaxy, unconditionally energy stable, finite difference schemes, adaptive time-stepping method

AMS subject classifications. 35Q99, 35R99, 65M12, 65M70

DOI. 10.1137/100812781

1. Introduction.

There has been a significant amount of research in the dynamics of the molecular beam epitaxy (MBE) growth. Different kinds of models have been developed, which typically include atomistic models, continuum models, and hybrid models; see, e.g. [3, 4, 14]. In this work, we are interested in the continuum model for the evolution of the MBE growth with the isotropic symmetry current, which is governed by the following partial differential equation:

$$\frac{\partial \phi}{\partial t} = -\epsilon \Delta^2 \phi - \nabla \cdot [(1 - |\nabla \phi|^2) \nabla \phi], \quad (\mathbf{x}, t) \in \Omega \times (0, T], \tag{1.1}$$

where $\phi = \phi(\mathbf{x}, t)$ is a scaled height function of a thin film in a comoving frame and ϵ is a positive constant; $\Omega = (0, L)^2$ with $L > 0$. The fourth-order term models surface diffusion, and the nonlinear second-order term models the Ehrlich–Schwoebel effect. The growth equation (1.1) is the gradient flow with respect to the $L^2(\Omega)$ inner product of the energy functional

$$E(\phi) = \int_\Omega \left[\frac{1}{4} (|\nabla \phi|^2 - 1)^2 + \frac{\epsilon}{2} |\Delta \phi|^2 \right] d\mathbf{x}. \tag{1.2}$$

This form of energy often appears in several areas of material modeling. For instance, it serves as a variational model in the theory of liquid crystals [1]. It is an example

*Submitted to the journal's Methods and Algorithms for Scientific Computing section October 25, 2010; accepted for publication (in revised form) April 11, 2011; published electronically June 14, 2011.

http://www.siam.org/journals/sisc/33-3/81278.html

†Department of Mathematics, Hong Kong Baptist University, Kowloon, Hong Kong (zqiao@hkbu.edu.hk, ttang@hkbu.edu.hk). The research of the first author was supported by the FRG grants of the Hong Kong Baptist University under grant FRG/08-09/II-35. The research of the third author was supported by the Hong Kong Research Grants Council and by the Collaborative Research Fund of National Science Foundation of China (NSFC) under grant G10729101.

‡Corresponding author. School of Mathematical Sciences, Beijing Normal University, Beijing, 100875, China (zrzhang@bnu.edu.cn). The research of this author was supported by National NSF of China under grant 10601007.

of elastic energy functional of scalar deformations h in the strain-gradient theory for structural phase transitions in solids [2, 11]. It is also a simplified and rescaled folding energy for an out-of-plane displacement h modeling the folding pattern of a blister formed in the buckling-driven delamination of thin films [8, 10].

The other MBE growth model we are interested in is the one with square surface current

$$\frac{\partial \phi}{\partial t} = -\epsilon \Delta^2 \phi - \left((1-|\phi_x|^2)\phi_x\right)_x - \left((1-|\phi_y|^2)\phi_y\right)_y, \quad (\mathbf{x},t) \in \Omega \times (0,T]. \tag{1.3}$$

The energy functional corresponding to MBE model (1.3) is

$$\widetilde{E}(\phi) = \int_\Omega \left\{ \frac{\epsilon}{2}|\Delta\phi|^2 + \frac{1}{4}[(\phi_x^2-1)^2 + (\phi_y^2-1)^2] \right\} d\mathbf{x}. \tag{1.4}$$

Both models (1.1) and (1.3) are subject to the periodic boundary conditions and suitable initial data.

In [19], a semi-implicit first-order scheme was proposed for solving the phase field crystal equation of sixth-order derivative. The unconditionally energy stability was proved based on the convex splitting of the energy functional. In [20], an implicit-explicit approach for solving the MBE growth models was presented and the analysis on energy stability was also studied, where the nonlinear term is treated explicitly. It is demonstrated that by adding some linear terms consistent with the truncation errors in time the stability is guaranteed. However, the artificial term depends on the unknown numerical solutions. A similar technique was used by Zhu, Chen, and Tikare [21] in the simulation of the Cahn–Hilliard equation. In this work, we will first propose two semi-implicit schemes; one handles the diffusion term explicitly using the known previous data, and the other uses the Crank–Nicolson (C-N) type implicit approximation. For both schemes, we can prove that the energy decay is preserved without introducing any artificial terms (compare [9, 20]). The C-N type implicit scheme uses a special combination of the nonlinear term. Such a combination has been used in [5] for a fully discretized scheme of the one dimensional Cahn–Hilliard equations. The energy decay and pointwise bounds of discrete solutions of the Cahn–Hilliard equation were obtained in that paper.

Adaptive time stepping has been well studied for solving initial value problems in ODEs. Söderlind [17] reviewed some time step control methods for local time adaptivity based on linear feedback theory. In [14], two adaptive time methods are compared with constant time steps for coupled flow and deformation models. In their work, the pore pressure method is an inexpensive adaptive method whose behavior closely follows the physics of the problem, while the local error method is more time-consuming at each time step because feedback steps may be involved. In [18], a locally varying time step method was developed for solving hyperbolic conservative PDEs. At the same time level, large time step is adopted on domain with smooth solution, while small time step is taken in the region with nearly singular solutions. In this work, our adaptive time-stepping technique will be developed based on the energy variation, which is an important physical quantity in the MBE growth model.

The main objective of this work includes two parts: First, we will propose two second-order implicit schemes for solving MBE models. The linear second order diffusion term is treated using either extrapolation or C-N type approximations. Second, we will develop an adaptive time-stepping technique, which is very effective for a class of evolutionary equations with the so-called "rough-smooth-rough" growth pattern and long time simulations. In the time interval with rapid energy decay, small

time steps are chosen adaptively, while in the time interval with very smooth energy variation, large time steps are used. With automatic selection of time steps, the computational efficiency can be improved significantly. In our computations, Newton-multigrid iterative method is used to solve the system with good initial guess at each iterative step.

In [12], the stability of the weak solution of the MBE model is studied. Relevant works have been done for the Cahn–Hilliard and Allen–Cahn phase field equations, see, e.g., [6, 7]. the authors also studied numerical stability. The stability of these works is in the classical sense, i.e., continuous dependence of solutions on the initial conditions. In this work, both kinds of stability are considered: energy stability and the classical initial data-dependence stability.

This paper is organized as follows. In section 2, we construct two second-order unconditionally energy stable implicit finite difference methods for solving the MBE model equations. The proposed schemes allow arbitrarily large time steps and, therefore, are very useful for long time simulations. An adaptive time-stepping technique is proposed in section 3, where the adaptive time step is determined based on the variation of the energy. Numerical experiments are presented in section 4, and some concluding remarks are given in the final section.

2. Semi-implicit scheme with second-order in time. In order to analyze the numerical stability, we first state the following known results for the continuum MBE models.

LEMMA 2.1 (energy identities [12]). *If $\phi(\mathbf{x},t)$ is a solution of the MBE model* (1.1), *then the following energy identities hold:*

$$\frac{d}{dt}\|\phi\|^2 + 4E(\phi) + \|\nabla\phi\|_{L^4}^4 = |\Omega|, \tag{2.1}$$

$$\frac{d}{dt}E(\phi) + \|\phi_t\|^2 = 0, \tag{2.2}$$

where $\|\cdot\|$ is the standard L^2-norm in Ω, L^p is the standard L^p-norm, and the energy functional is defined in (1.2).

The brief proof for this lemma is as follows. From (1.1), we can easily get

$$\left(\frac{\partial\phi}{\partial t},\varphi\right) = -(\nabla\cdot[(1-|\nabla\phi|^2)\nabla\phi + \epsilon\nabla\Delta\phi],\varphi), \tag{2.3}$$

where $(\cdot,\cdot)$ denotes the standard inner product in the L^2-space. Setting $\varphi = \phi$ and considering the periodic boundary condition for ϕ gives (2.1), and setting $\varphi = \phi_t$ leads to (2.2).

LEMMA 2.2. *The solution $\phi(\mathbf{x},t)$ of* (1.1) *is L^2 stable with respect to the initial condition:*

$$\|\phi(\cdot,t)\|^2 \le e^{t/(2\epsilon)}\|\phi(\cdot,0)\|^2. \tag{2.4}$$

In (2.3), setting $\varphi = \phi$ and after a careful estimate including Green's formula, and Cauchy–Schwarz inequality we can get the above result.

Similar to the proof of the above two lemmas, we can obtain the following results.

LEMMA 2.3. *If $\phi(\mathbf{x},t)$ is a solution of the MBE model* (1.3)*, then the following energy identities hold:*

$$\frac{d}{dt}\|\phi\|^2 + 4\bar{E}(\phi) + \|\phi_x\|_{L^4}^4 + \|\phi_y\|_{L^4}^4 = 2|\Omega|, \tag{2.5}$$

$$\frac{d}{dt}\bar{E}(\phi) + \|\phi_t\|^2 = 0. \tag{2.6}$$

LEMMA 2.4. *The solution $\phi(\mathbf{x},t)$ of* (1.3) *is L^2-stable with respect to the initial condition:*

$$\|\phi(\cdot,t)\|^2 \le e^{t/(2\epsilon)}\|\phi(\cdot,0)\|^2. \tag{2.7}$$

2.1. A second-order scheme: Extrapolation for diffusion term. In [19], a second-order finite difference scheme is proposed to solve the phase field crystal equation, where the diffusion term $\Delta\phi$ is approximated using extrapolation. Following [19], we can give a second-order scheme for the MBE model (1.1):

$$frac\phi_{j,k}^{n+1} - \phi_{j,k}^{n}\Delta t = -\nu_{j,k}^{n+\frac{1}{2}}, \tag{2.8}$$

with

$$\nu_{j,k}^{n+\frac{1}{2}} = \epsilon\frac{\Delta_h^2\phi_{j,k}^{n+1} + \Delta_h^2\phi_{j,k}^{n}}{2} - \nabla_h\cdot\left(\frac{|\nabla_h\phi_{j,k}^{n+1}|^2 + |\nabla_h\phi_{j,k}^{n}|^2}{2}\frac{\nabla_h\phi_{j,k}^{n+1} + \nabla_h\phi_{j,k}^{n}}{2}\right) + \left(\frac{3\Delta_h\phi_{j,k}^{n}}{2} - \frac{\Delta_h\phi_{j,k}^{n-1}}{2}\right),$$

where $\phi_{j,k}^{n+1}$ are subject to periodic boundary conditions, ∇_h and Δ_h are central-scheme operators of the finite difference method, and h is the mesh size of the space discretizition. For the case $n=0$, we set $\phi^{-1}=\phi^0$. This choice of the initialization will give the first-order accuracy for the first time step. However, we can use a smaller Δt at the beginning of the time evolution which helps to keep the overall accuracy.

THEOREM 2.1. *Let $\{\phi_{j,k}^n\}$ be the numerical solution of* (2.8) *at t_n. Then we have*

$$\|\phi^n\|_h^2 \le C_1\|\phi^0\|_h^2, \quad 1\le n\le N, \tag{2.9}$$

where $\|\cdot\|_h$ denotes the discrete L^2-norm; C_1 is independent of Δt and h, but depends on $1/\epsilon$.

Proof. Multiplying (2.8) by $(\phi_{j,k}^{n+1}+\phi_{j,k}^{n})/2$ and summing for $j=1,\dots,N_x$ and $k=1,\dots,N_y$, we get

$$\begin{aligned}\frac{1}{2\Delta t}\left(\|\phi^{n+1}\|_h^2 - \|\phi^n\|_h^2\right) + \epsilon\left\|\frac{\Delta_h(\phi^{n+1}+\phi^n)}{2}\right\|_h^2 \\ - \left(\nabla_h\cdot\left(\frac{|\nabla_h\phi^{n+1}|^2 + |\nabla_h\phi^{n}|^2}{2}\frac{\nabla_h\phi^{n+1} + \nabla_h\phi^{n}}{2}\right), \frac{\phi^{n+1}+\phi^n}{2}\right)_h \\ + \left(\frac{3\Delta_h\phi^n}{2} - \frac{\Delta_h\phi^{n-1}}{2}, \frac{\phi^{n+1}+\phi^n}{2}\right)_h = 0,\end{aligned} \tag{2.10}$$

where $(\cdot,\cdot)_h$ denotes the discrete L^2 inner product. By Green's formula, the above equation becomes

$$\begin{aligned}(2.11)\quad &\frac{1}{2\Delta t}\left(\|\phi^{n+1}\|_h^2-\|\phi^n\|_h^2\right)+\epsilon\left\|\frac{\Delta_h(\phi^{n+1}+\phi^n)}{2}\right\|_h^2\\ &\quad+\left(\frac{|\nabla_h\phi^{n+1}|^2+|\nabla_h\phi^n|^2}{2},\frac{|\nabla_h\phi^{n+1}+\nabla_h\phi^n|^2}{2}\right)_h\\ &\qquad=-\left(\frac{3}{2}\phi^n-\frac{1}{2}\phi^{n-1},\frac{\Delta_h\phi^{n+1}+\Delta_h\phi^n}{2}\right)_h.\end{aligned}$$

Neglecting the third positive term on the left-hand side, we get

$$\begin{aligned}(2.12)\qquad &\frac{1}{2\Delta t}\left(\|\phi^{n+1}\|_h^2-\|\phi^n\|_h^2\right)+\epsilon\left\|\frac{\Delta_h(\phi^{n+1}+\phi^n)}{2}\right\|_h^2\\ &\quad\le\left|\left(\frac{3\phi^n}{2}-\frac{\phi^{n-1}}{2},\Delta_h\frac{\phi^{n+1}+\phi^n}{2}\right)_h\right|\\ &\quad\le\epsilon\left\|\frac{\Delta_h(\phi^{n+1}+\phi^n)}{2}\right\|_h^2+\frac{1}{4\epsilon}\left\|\frac{3\phi^n}{2}-\frac{\phi^{n-1}}{2}\right\|_h^2.\end{aligned}$$

It follows that

$$\begin{aligned}(2.13)\qquad &\frac{1}{2\Delta t}\Big(\|\phi^{n+1}\|_h^2-\|\phi^n\|_h^2\Big)\le\frac{1}{4\epsilon}\left\|\frac{3\phi^n}{2}-\frac{\phi^{n-1}}{2}\right\|_h^2\\ &\qquad\le\frac{1}{8\epsilon}\Big(9\|\phi^n\|_h^2+\|\phi^{n-1}\|_h^2\Big).\end{aligned}$$

Summing both sides with respect to n gives

$$\|\phi^{n+1}\|_h^2\le\|\phi^0\|_h^2+\frac{\Delta t}{4\epsilon}\sum_{k=0}^{n-1}\Big(9\|\phi^{k+1}\|_h^2+\|\phi^k\|_h^2\Big).$$

Then the Gronwall inequality yields

$$\|\phi^{n+1}\|_h^2\le C_1\|\phi^0\|_h^2,$$

where the constant C_1 is independent of h and Δt. ∎

THEOREM 2.2. *The semi-implicit fully discrete scheme* (2.8) *is unconditionally energy stable with respect to the initial energy. More precisely, for any time step* $\Delta t>0$, *there holds*

$$(2.14)\qquad E_h(\phi^n)\le E_h(\phi^0),$$

where ϕ^n *denotes the numerical solution of* (2.8) *at* t_n *and* E_h *is the discrete form of the energy functional* (1.2).

Proof. Multiplying (2.8) by $h^2\nu_{j,k}^{n+\frac{1}{2}}$ and summing for $j=1,\dots,N_x$ and $k=1,\dots,N_y$, we get

$$(2.15)\qquad -\Delta t\|\nu^{n+\frac{1}{2}}\|_h^2=(\nu^{n+\frac{1}{2}},\phi^{n+1}-\phi^n)_h.$$

Straightforward computations for the right-hand side above yield

$$\begin{aligned}
&(\nu^{n+\frac{1}{2}}, \phi^{n+1}-\phi^n)_h \\
&\quad = \frac{\epsilon}{2}\|\Delta_h\phi^{n+1}\|_h^2 - \frac{\epsilon}{2}\|\Delta_h\phi^n\|_h^2 \\
&\qquad + \left(\phi^{n+1}-\phi^n, -\nabla_h\cdot\left(\frac{|\nabla_h\phi^{n+1}|_h^2+|\nabla_h\phi^n|_h^2}{2}\frac{\nabla_h\phi^{n+1}+\nabla_h\phi^n}{2}\right)\right)_h \\
&\qquad + \left(\phi^{n+1}-\phi^n, \frac{3\Delta_h\phi^n}{2}-\frac{\Delta_h\phi^{n-1}}{2}\right)_h \\
&\quad = \frac{\epsilon}{2}\|\Delta_h\phi^{n+1}\|_h^2 - \frac{\epsilon}{2}\|\Delta_h\phi^n\|_h^2 + \left(\frac{|\nabla_h\phi^{n+1}|^4}{4}-\frac{|\nabla_h\phi^n|^4}{4}, 1\right)_h \\
&\qquad + \left(\phi^{n+1}-\phi^n, \frac{3\Delta_h\phi^n}{2}-\frac{\Delta_h\phi^{n-1}}{2}\right)_h.
\end{aligned}$$

Using the definition of $E_h(\cdot)$, we obtain

$$\begin{aligned}
&(\nu^{n+\frac{1}{2}}, \phi^{n+1}-\phi^n)_h \\
&\quad = E_h(\phi^{n+1}) - E_h(\phi^n) + \frac{1}{2}\|\nabla_h\phi^{n+1}\|_h^2 - \frac{1}{2}\|\nabla_h\phi^n\|_h^2 \\
&\qquad + \left(\phi^{n+1}-\phi^n, \frac{3\Delta_h\phi^n}{2}-\frac{\Delta_h\phi^{n-1}}{2}\right)_h \\
&\quad = E_h(\phi^{n+1}) - E_h(\phi^n) + \frac{1}{2}\|\nabla_h\phi^{n+1}\|_h^2 - \frac{1}{2}\|\nabla_h\phi^n\|_h^2 \\
&\qquad - \frac{1}{2}\left(\nabla_h(\phi^{n+1}-\phi^n), \nabla_h(\phi^n-\phi^{n-1})\right)_h \\
&\qquad - \frac{1}{2}\|\nabla_h\phi^{n+1}\|_h^2 + \frac{1}{2}\|\nabla_h\phi^n\|_h^2 + \frac{1}{2}\|\nabla_h(\phi^{n+1}-\phi^n)\|_h^2.
\end{aligned} \tag{2.16}$$

Combining (2.16) and (2.15) leads to

$$\begin{aligned}
&E_h(\phi^{n+1}) - E_h(\phi^n) \\
&\quad = -\Delta t\|\nu^{n+\frac{1}{2}}\|_h^2 - \frac{1}{2}\|\nabla_h(\phi^{n+1}-\phi^n)\|_h^2 \\
&\qquad + \frac{1}{2}\left(\nabla_h(\phi^{n+1}-\phi^n), \nabla_h(\phi^n-\phi^{n-1})\right)_h \\
&\quad \le -\Delta t\|\nu^{n+\frac{1}{2}}\|_h^2 - \frac{1}{4}\|\nabla_h(\phi^{n+1}-\phi^n)\|_h^2 + \frac{1}{4}\|\nabla_h(\phi^n-\phi^{n-1})\|_h^2.
\end{aligned} \tag{2.17}$$

Then the last term in the above inequality disappears. Summing both sides with respect to n gives

$$E_h(\phi^n) \le E_h(\phi^0) - \Delta t\sum_{k=0}^{n-1}\|\nu^{k+\frac{1}{2}}\|_h^2 - \frac{1}{4}\|\nabla_h(\phi^k-\phi^{k-1})\|_h^2,$$

which leads to (2.14). □

Let us make some further discussions on Theorem 2.2. Define a new discrete energy as below

$$F_h(\phi^n, \phi^{n-1}) = E_h(\phi^n) + \frac{1}{4}\|\nabla_h(\phi^n-\phi^{n-1})\|_h^2.$$

Then it follows from (2.17) that

$$F_h(\phi^{n+1},\phi^n) \le F_h(\phi^n,\phi^{n-1}).$$

It is noted that

$$F_h(\phi^n,\phi^{n-1}) \to E_h(\phi^n) \quad \text{as} \quad \Delta t \to 0.$$

Consequently, the energy F_h is consistent with the original energy E_h as $\Delta t \to 0$.

2.2. Crank–Nicolson scheme. The second-order Crank–Nicolson scheme for the MBE model with symmetric current (1.1) is of the form

$$\frac{\phi_{j,k}^{n+1}-\phi_{j,k}^n}{\Delta t} \equiv -\mu_{j,k}^{n+\frac{1}{2}}, \tag{2.18}$$

with

$$\mu_{j,k}^{n+\frac{1}{2}} = \epsilon\frac{\Delta_h^2\phi_{j,k}^{n+1}+\Delta_h^2\phi_{j,k}^n}{2} - \nabla_h\cdot\left(\frac{|\nabla_h\phi_{j,k}^{n+1}|^2+|\nabla_h\phi_{j,k}^n|^2}{2}\frac{\nabla_h\phi_{j,k}^{n+1}+\nabla_h\phi_{j,k}^n}{2}\right)+\left(\frac{\Delta_h\phi_{j,k}^{n+1}}{2}+\frac{\Delta_h\phi_{j,k}^n}{2}\right),$$

where $\phi_{j,k}^{n+1}$ are subject to periodic boundary conditions. Here, the diffusion term $\Delta\phi$ is treated implicitly rather than using extrapolation.

THEOREM 2.3. *Let $\{\phi_{j,k}^n\}$ be the numerical solution of* (2.18) *at t_n. Then we have*

$$\|\phi^n\|_h^2 \le C_2\|\phi^0\|_h^2, \quad 1\le n\le N \tag{2.19}$$

provided that $\Delta t < 4\epsilon$, where C_2 is independent of h and Δt, but depends on $1/\epsilon$.

Proof. Multiplying (2.18) by $(\phi_{j,k}^{n+1}+\phi_{j,k}^n)/2$ and summing for $j=1,\dots,N_x$ and $k=1,\dots,N_y$ yield

$$\begin{aligned}\frac{1}{2\Delta t}\left(\|\phi^{n+1}\|_h^2-\|\phi^n\|_h^2\right)+\epsilon\left\|\frac{\Delta_h(\phi^{n+1}+\phi^n)}{2}\right\|_h^2 \\ +\left(-\nabla_h\cdot\left(\frac{|\nabla_h\phi^{n+1}|^2+|\nabla_h\phi^n|^2}{2}\frac{\nabla_h\phi^{n+1}+\nabla_h\phi^n}{2}\right),\frac{\phi^{n+1}+\phi^n}{2}\right)_h \\ +\left(\frac{\Delta_h(\phi^{n+1}+\phi^n)}{2},\frac{\phi^{n+1}+\phi^n}{2}\right)_h=0.\end{aligned} \tag{2.20}$$

By use of Green's formula, the above equation becomes

$$\begin{aligned}\frac{1}{2\Delta t}(\|\phi^{n+1}\|_h^2-\|\phi^n\|_h^2)+\epsilon\left\|\frac{\Delta_h(\phi^{n+1}+\phi^n)}{2}\right\|_h^2 \\ +\left(\frac{|\nabla_h\phi^{n+1}|^2+|\nabla_h\phi^n|^2}{2},\frac{|\nabla_h\phi^{n+1}+\nabla_h\phi^n|^2}{2}\right)_h \\ =\left\|\frac{\nabla_h(\phi^{n+1}+\phi^n)}{2}\right\|_h^2.\end{aligned} \tag{2.21}$$

Neglecting the third positive term on the left-hand side, we get

$$\begin{aligned}\frac{1}{2\Delta t}\left(\|\phi^{n+1}\|_h^2-\|\phi^n\|_h^2\right)+\epsilon\left\|\frac{\Delta_h(\phi^{n+1}+\phi^n)}{2}\right\|_h^2 &\le \left\|\frac{\nabla_h(\phi^{n+1}+\phi^n)}{2}\right\|_h^2\\ &\le \epsilon\left\|\frac{\Delta_h(\phi^{n+1}+\phi^n)}{2}\right\|_h^2+\frac{1}{4\epsilon}\left\|\frac{\phi^{n+1}+\phi^n}{2}\right\|_h^2,\end{aligned} \tag{2.22}$$

which leads to

$$\begin{aligned}\frac{1}{2\Delta t}\left(\|\phi^{n+1}\|_h^2-\|\phi^n\|_h^2\right) &\le \frac{1}{4\epsilon}\left\|\frac{\phi^{n+1}+\phi^n}{2}\right\|_h^2\\ &\le \frac{1}{8\epsilon}\Big(\|\phi^{n+1}\|_h^2+\|\phi^n\|_h^2\Big).\end{aligned} \tag{2.23}$$

Summing both sides with respect to n gives

$$\Big(1-\frac{\Delta t}{4\epsilon}\Big)\|\phi^{n+1}\|_h^2 \le \|\phi^0\|_h^2+\frac{\Delta t}{2\epsilon}\sum_{k=0}^{n}\|\phi^k\|_h^2.$$

When $\Delta t<4\epsilon$, the Gronwall inequality yields

$$\|\phi^n\|_h^2 \le C_2\|\phi^0\|_h^2,$$

where C_2 is a general constant independent of h and Δt. ∎

THEOREM 2.4. *The semi-implicit fully discrete scheme* (2.18) *is unconditionally energy stable. More preciously, for any time step $\Delta t>0$, we have*

$$E_h(\phi^{n+1}) \le E_h(\phi^n),$$

where E_h is the discrete form of the energy functional (1.2). *Furthermore, the discrete form of the energy identity* (2.2) *holds:*

$$\frac{E_h(\phi^{n+1})-E_h(\phi^n)}{\Delta t}+\left\|\frac{\phi^{n+1}-\phi^n}{\Delta t}\right\|_h^2=0, \tag{2.24}$$

where ϕ^n denotes the numerical solution of (2.18) *at t_n.*

Proof. Multiplying (2.18) by $h^2\mu_{j,k}^{n+\frac{1}{2}}$ and summing for $j=1,\dots,N_x$ and $k=1,\dots,N_y$, we get

$$-\Delta t\|\mu^{n+\frac{1}{2}}\|_h^2=(\mu^{n+\frac{1}{2}},\phi^{n+1}-\phi^n)_h. \tag{2.25}$$

It can be verified that the right-hand side above becomes

$$
\begin{aligned}
(2.26)\quad & (\mu^{n+\frac{1}{2}}, \phi^{n+1}-\phi^n)_h \\
&= \frac{\epsilon}{2}\|\Delta_h\phi^{n+1}\|_h^2 - \frac{\epsilon}{2}\|\Delta_h\phi^n\|_h^2 \\
&\quad + \left(\phi^{n+1}-\phi^n, -\nabla_h\cdot\left(\frac{|\nabla_h\phi^{n+1}|_h^2+|\nabla_h\phi^n|_h^2}{2}\frac{\nabla_h\phi^{n+1}+\nabla_h\phi^n}{2}\right)\right) \\
&\quad + \left(\phi^{n+1}-\phi^n, \frac{\Delta_h\phi^{n+1}}{2}+\frac{\Delta_h\phi^n}{2}\right)_h \\
&= \frac{\epsilon}{2}\|\Delta_h\phi^{n+1}\|_h^2 - \frac{\epsilon}{2}\|\Delta_h\phi^n\|_h^2 + \left(\frac{|\nabla_h\phi^{n+1}|^4}{4}-\frac{|\nabla_h\phi^n|^4}{4}, 1\right)_h \\
&\quad -\frac{1}{2}\left(\nabla_h(\phi^{n+1}-\phi^n), \nabla_h(\phi^{n+1}+\phi^n)\right)_h \\
&= E_h(\phi^{n+1}) - E_h(\phi^n).
\end{aligned}
$$

Combining (2.26) and (2.25) leads to

$$
E_h(\phi^{n+1}) - E_h(\phi^n) = -\Delta t\|\mu^{n+\frac{1}{2}}\|_h^2, \tag{2.27}
$$

which gives

$$
\frac{E_h(\phi^{n+1})-E_h(\phi^n)}{\Delta t} = -\|\mu^{n+\frac{1}{2}}\|_h^2 = -\left\|\frac{\phi^{n+1}-\phi^n}{\Delta t}\right\|_h^2. \tag{2.28}
$$

This suggests that the proposed second-order scheme (2.18) satisfies the unconditional energy stability condition exactly. ∎

Similar to the scheme (2.8), the MBE model with square symmetric surface (1.3) can be approximated by

$$
\begin{aligned}
(2.29)\quad & \frac{\phi_{j,k}^{n+1}-\phi_{j,k}^n}{\Delta t} \\
&= -\epsilon\left(\frac{\Delta_h^2\phi_{j,k}^{n+1}+\Delta_h^2\phi_{j,k}^n}{2}\right) \\
&\quad + \delta_x\left(\frac{|(\delta_x\phi)_{j,k}^{n+1}|^2+|(\delta_x\phi)_{j,k}^n|^2}{2}\frac{(\delta_x\phi)_{j,k}^{n+1}+(\delta_x\phi)_{j,k}^n}{2}\right)_{j,k} \\
&\quad + \delta_y\left(\frac{|(\delta_y\phi)_{j,k}^{n+1}|^2+|(\delta_y\phi)_{j,k}^n|^2}{2}\frac{(\delta_y\phi)_{j,k}^{n+1}+(\delta_y\phi)_{j,k}^n}{2}\right)_{j,k} \\
&\quad - \left(\frac{3\Delta_h\phi_{j,k}^n}{2}-\frac{\Delta_h\phi_{j,k}^{n-1}}{2}\right),
\end{aligned}
$$

where δ_x, δ_y are central difference operators.

For the scheme (2.29), we have the following results about stability.

THEOREM 2.5. *Suppose that $\{\phi_{j,k}^n\}$ is the solution of* (2.29) *at t_n. We have the following results:*

(i) *The numerical scheme* (2.29) *is L^2-stable with respect to the initial condition*

$$
\|\phi^n\|_h^2 \le \bar{C}_1\|\phi^0\|_h^2,
$$

where $\bar{C}_1$ is a positive constant independent of h and Δt, but depends on $1/\epsilon$.

(ii) *The numerical scheme* (2.29) *is unconditionally energy stable with respect to the initial energy in the sense that*

$$\bar{E}_h(\phi^n) \le \bar{E}_h(\phi^0),$$

where $\bar{E}_h$ *is defined as the discrete form of the energy functional* (1.4). *Moreover, we have*

$$\bar{F}_h(\phi^{n+1}, \phi^n) \le \bar{F}(\phi^n, \phi^{n-1}),$$

where $\bar{F}_h$ *is defined by*

$$\bar{F}_h(\phi^n, \phi^{n-1}) = \bar{E}_h(\phi^n) + \frac{1}{4}\|\nabla_h(\phi^n - \phi^{n-1})\|_h^2,$$

which is convergent to the original energy $\bar{E}_h(\phi^n)$ *as* $\Delta t \to 0$.

Similarly, for the MBE growth model with square symmetric surface (1.3), the C-N scheme is of the form

$$\begin{aligned}
&\frac{\phi_{j,k}^{n+1} - \phi_{j,k}^n}{\Delta t} \\
&= -\epsilon \left(\frac{\Delta_h^2 \phi_{j,k}^{n+1} + \Delta_h^2 \phi_{j,k}^n}{2} \right) \\
&\quad + \delta_x \left(\frac{|(\delta_x \phi)_{j,k}^{n+1}|^2 + |(\delta_x \phi)_{j,k}^n|^2}{2} \frac{(\delta_x \phi)_{j,k}^{n+1} + (\delta_x \phi)_{j,k}^n}{2} \right)_{j,k} \\
&\quad + \delta_y \left(\frac{|(\delta_y \phi)_{j,k}^{n+1}|^2 + |(\delta_y \phi)_{j,k}^n|^2}{2} \frac{(\delta_y \phi)_{j,k}^{n+1} + (\delta_y \phi)_{j,k}^n}{2} \right)_{j,k} \\
&\quad - \left(\frac{\Delta_h \phi_{j,k}^{n+1}}{2} + \frac{\Delta_h \phi_{j,k}^n}{2} \right).
\end{aligned} \tag{2.30}$$

We have the following stability results.

THEOREM 2.6. *Suppose that* $\{\phi_{j,k}^n\}$ *is the solution of* (2.30) *at* t_n. *We have the following results:*

(i) *The numerical scheme* (2.30) *is* L^2*-stable with respect to the initial condition*

$$\|\phi^n\|_h^2 \le \bar{C}_2 \|\phi^0\|_h^2,$$

where $\bar{C}_2$ *is independent of* h *and* Δt, *but depends on* $1/\epsilon$.

(ii) *The numerical scheme* (2.30) *is unconditionally energy stable:*

$$\bar{E}_h(\phi^{n+1}) \le \bar{E}_h(\phi^n).$$

Furthermore, the discrete form of the energy identity (2.6) *holds:*

$$\frac{\bar{E}_h(\phi^{n+1}) - \bar{E}_h(\phi^n)}{\Delta t} + \left\| \frac{\phi^{n+1} - \phi^n}{\Delta t} \right\|_h^2 = 0.$$

The proofs for Theorems 2.5 and 2.6 are similar to those for Theorems 2.1–2.4.

Both of the finite difference schemes (2.8) and (2.18) give nonlinear systems, which will be solved by using the Newton iteration method. The initial guess for the Newton iteration at the time level t_{n+1} is taken as the numerical solution at the previous time level t_n. At each Newton iteration step, the algebraic multigrid method is employed to solve the linear system.

3. Adaptive time stepping. In the previous sections, we have proved that (2.8) and (2.18) are unconditionally energy stable. It will allow us to apply large time steps during the numerical simulations. For the sake of accuracy, a very large time step is unacceptable except in the time intervals where the solution variation is very small. Our numerical experiments also show that long time simulations using large constant time steps may produce nonphysical solutions at intermediate time stages (i.e., wrong dynamics), although the steady-state behaviors are less sensitive to the time steps used. It is known from the experiments and the perturbation analysis that the MBE growth follows a rough-smooth-rough pattern. At the early stage of the thin film epitaxy, the corresponding energy decays quickly because of the nonlinear interaction, and then the energy decays rather slowly until it reaches a steady state. Based on these observations, we are motivated to adjust time steps using the following form:

$$\Delta t = \max\left(\Delta t_{\min}, \frac{\Delta t_{\max}}{\sqrt{1+\alpha|E'(t)|^2}}\right), \quad \alpha = \text{const}, \tag{3.1}$$

where E is the energy functional defined in (1.2) (or (1.4) for the model (1.3)).

Let $\mathrm{w}(t)$ be the roughness (or the interface width) for the the height function at time t defined as

$$\mathrm{w}(t) = \sqrt{\frac{1}{|\Omega|}\int_\Omega [\phi(\mathbf{x},t) - \bar{\phi}(t)]^2 d\mathbf{x}}, \quad \text{where} \quad \bar{\phi}(t) = \frac{1}{|\Omega|}\int_\Omega \phi(\mathbf{x},t) d\mathbf{x}$$

and $|\Omega|$ denotes the area of the domain. It is known that $|E'(t)|$ in (3.1) may be replaced by $|\mathrm{w}'(t)|$ because $|\mathrm{w}'(t)|$ and $|E'(t)|$ have similar behaviors throughout the MBE growth. The roughness-dependent adaptive time step is

$$\Delta t = \max\left(\Delta t_{\min}, \frac{\Delta t_{\max}}{\sqrt{1+\alpha|\mathrm{w}'(t)|^2}}\right), \quad \alpha = \text{const}. \tag{3.2}$$

The introduction of the preset smallest time step $\Delta t_{\min}$ is to force the adaptive time steps bounded below by $\Delta t_{\min}$. Likewise, $\Delta t_{\max}$ gives the upper bound of the time steps. Consequently,

$$\Delta t_{\min} \le \Delta t \le \Delta t_{\max}. \tag{3.3}$$

Moreover, large $|E'(t)|$ will lead to small time step, which corresponds to the case of rapid decay of energy or quick motion of the quick structural transition from one stage to the immediate next one. Similarly, small $|E'(t)|$ yields large time step, which corresponds to the slow motion of the MBE growth between the consecutive two stages. $\Delta t_{\min}$ is relevant to most rapid energy decay, and $\Delta t_{\max}$ corresponds to the slowest energy decay.

$\Delta t_{\min}$ and $\Delta t_{\max}$ are used to avoid using too small and too large time steps, respectively. This has been the practice in the adaptive time-stepping study for solving ordinary differential equations; see, e.g., [17]. A more involving parameter in our adaptive strategy is α. Choosing this α properly is also an issue in arclength related monitor functions of moving mesh methods for boundary value problems. One possible way to avoid the ad hoc approach may be the use of the error-estimator-based monitor; see, e.g. [13], which will be our future work.

4. Numerical experiments. In this section, we use the second-order scheme (2.18) to compute the MBE model (1.1). Both constant and adaptive time steps are employed to obtain numerical solutions. The adaptive time step is determined by (3.1). The tolerance of the Newton iteration method is set to be 10^{-6}, and the tolerance of the multigrid solver for solving linear system at each Newton iterative step is 10^{-8}.

Example 4.1. Consider the following one-dimensional MBE model problem

$$\phi_t = (\phi_x^3)_x - \phi_{xx} - \phi_{xxxx}, \qquad (x,t) \in (0,12) \times (0,T], \tag{4.1}$$

$$\phi(\cdot,t) \text{ is 12-periodic}, \qquad t \in [0,T], \tag{4.2}$$

$$\phi(x,0) = 0.1\Big(\sin\frac{\pi x}{2} + \sin\frac{2\pi x}{3} + \sin \pi x\Big), \qquad x \in [0,12]. \tag{4.3}$$

This one-dimensional initial-boundary-value problem has been studied in [12] to observe the morphological instability due to the nonlinear interaction. In order to test the numerical accuracy, we take the numerical solution obtained using second-order scheme (2.18) with a grid of $N = 200$ and constant time step $\Delta t = 10^{-4}$ as the "exact" solution at $t = 60$. The L^2-error is shown in Table 4.1. It is clearly observed that the C-N scheme (2.18) gives second-order accuracy in time.

TABLE 4.1
Example 4.1: L^2*-errors with different constant time steps,* $t = 60, N = 200$.

Δt	0.01	0.005	0.0025	0.00125
$\|e\|$	5.60E-3	1.63E-3	4.24E-4	1.05E-4

To further study the effect of the time step on the accuracy and stability of the numerical scheme, we use different constant time steps $\Delta t = 0.001, 0.01, 0.1$, and 1 to solve the MBE model (1.1). Since the numerical solution on the grid of $N = 100$ look quite similar as that on the grid of $N = 200$, we take $N = 100$ in the rest simulation of this example. In Figure 4.1(a), we show the numerical solution at $t = 40$. It is seen that only the solutions with $\Delta t \le 0.01$ are acceptable, while $\Delta t > 0.01$ will bring large numerical errors. Also we present the evolution of the energy in Figure 4.1(b). It is obvious that large time step $\Delta t = 1$ still gives correct solution of steady-state after a long time simulation, which is due to the unconditionally energy stablility. However, simulation with large time steps cannot catch the quick transient of the structure; see Figures 4.1(c) and Figure 4.1(d), which is caused by poor numerical accuracy in time.

We also studied the effectiveness of adaptive time-stepping techniques. Here, the time step is selected in the form of (3.1). We test different parameter settings $\Delta t_{\max} = 0.5, 1$ and $\Delta t_{\min} = 0.01$ with $\alpha = 10^5, 10^3$, and the numerical solution at $t = 40$ is plotted in Figure 4.2(a). It is observed that the adaptive time-stepping method with appropriate parameter settings can give satisfactory solutions. Also the energy evolution is shown in Figure 4.2(b). It is found that the adaptive time-stepping method can capture the solution structure throughout the evolution, especially for the structural transition stage; see Figures 4.2(c) and (d).

The corresponding time step development is presented in Figure 4.3. The time step is enlarged when $|E'(t)|$ becomes smaller. In the time intervals with quick energy decay, the time step becomes smaller. Once the solution reaches the steady-state, the derivative of energy becomes very small. Consequently, the time step approximates the upper bound $\Delta t_{\max}$. The parameter α in (3.1) is important determining satisfactory time steps. Here $\alpha = 10^5$ works well for this problem. We also tried $\alpha = 10^3$,

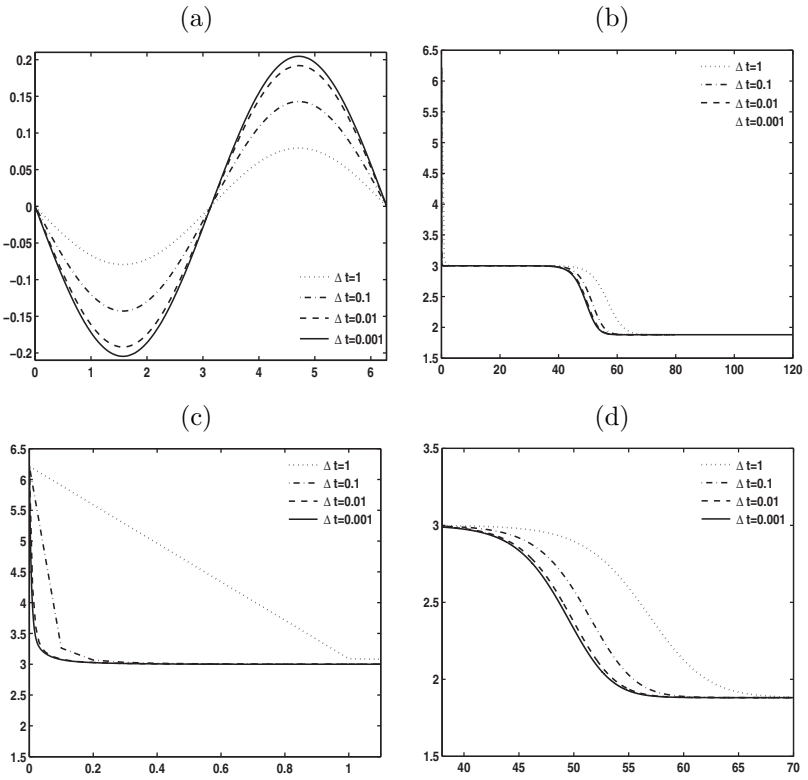

FIG. 4.1. *Example* 4.1: *Numerical solutions obtained using the C-N scheme and constant time steps* $\Delta t = 0.001, 0.01, 0.1, 1$. (a) *The numerical solution at* $t = 40$. (b) *Energy evolution,* $0 \le t \le 120$. (c) *Energy evolution at early stage,* $0 \le t \le 1.2$. (d) *Energy evolution at structure transient stage,* $38 \le t \le 70$.

which leads to relatively larger time steps and consequently solution transition is captured less accurately; see Figure 4.2.

Example 4.2. Consider the two-dimensional isotropic symmetry current model

$$\frac{\partial \phi}{\partial t} = -\epsilon \Delta^2 \phi - \nabla \cdot [(1 - |\nabla \phi|^2) \nabla \phi], \quad (\mathbf{x}, t) \in [0, 2\pi]^2 \times (0, T], \tag{4.4}$$

$$\phi(\mathbf{x}, 0) = \phi_0(\mathbf{x}), \quad \mathbf{x} \in [0, 2\pi]^2 \tag{4.5}$$

with 2π-periodic boundary condition and parameter $\epsilon = 0.1$. The initial condition is

$$\phi_0(\mathbf{x}) = 0.1(\sin 3x \sin 2y + \sin 5x \sin 5y).$$

This example was studied in [12, 20] to study the solution instability. Here we test the numerical accuracy and effectiveness of the adaptive time-stepping method for the second-order scheme (2.18). Since the exact solution is unknown, we take the numerical result obtained on a 200×200 grid and the time step $\Delta t = 0.0001$ as the "exact" solution. The solution contours at $t = 0.05$ and $t = 30$ (steady state) are plotted in Figure 4.4, which are in good agreement with the published ones in [12, 20]. Table 4.2 shows the L^2-errors obtained using different constant time steps. It is seen that for this two-dimensional MBE model problem the numerical scheme (2.18) gives $\mathcal{O}(\Delta t^2)$ error in time. Since the numerical solution on the 100×100 grid look quite

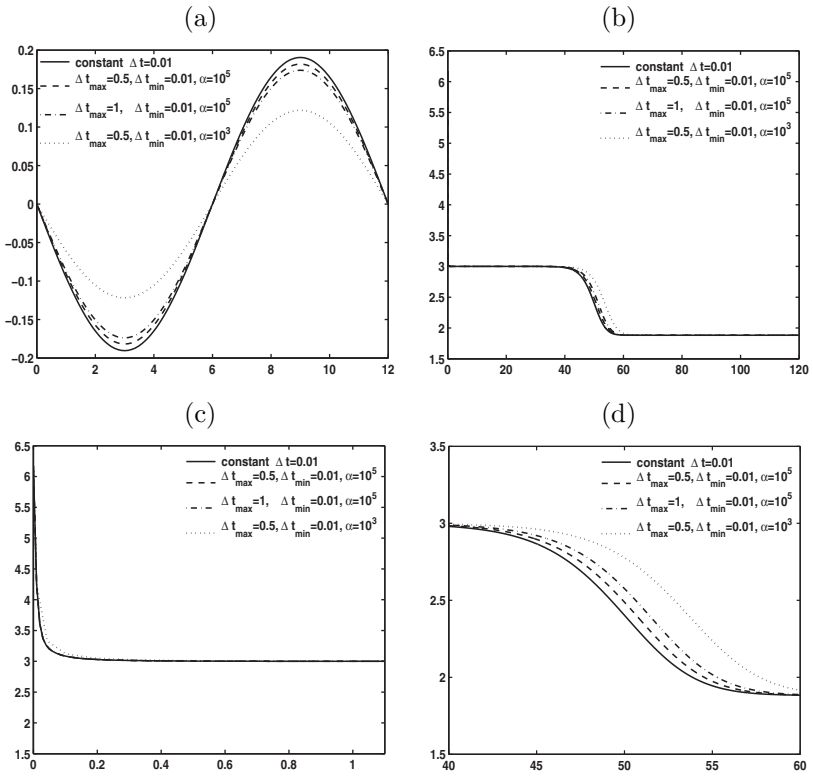

FIG. 4.2. *Example* 4.1: *Numerical solutions obtained using the C-N scheme and adaptive time steps with different parameters.* (a) *Numerical solution at* $t = 40$. (b) *Energy evolution evolution,* $0 \le t \le 120$. (c) *Energy evolution,* $0 \le t \le 1.2$. (d) *Energy evolution,* $40 \le t \le 60$.

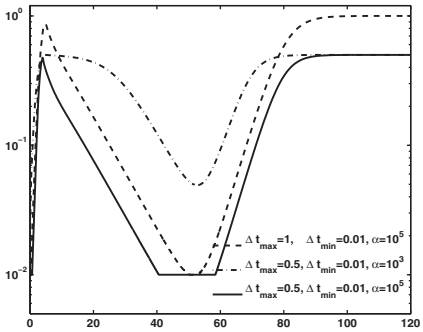

FIG. 4.3. *Example* 4.1: *Adaptive time step evolution.*

similar as that on the 200×200 grid, we use the 100×100 grid in the rest simulation of this example.

In order to test the numerical stability, we take different constant time steps to solve this MBE model. In our computation, it is found that using large time steps can produce correct steady-state solution. This is consistent with the discussion on unconditional energy stability in the previous section. However, the numerical solution at some intermediate stages may be incorrect due to large constant time steps used.

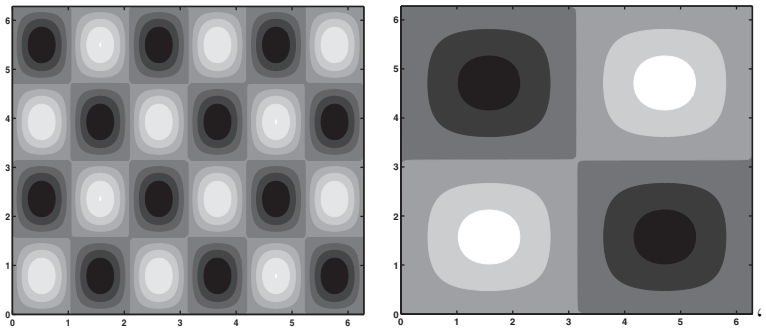

FIG. 4.4. *Example* 4.2: *Contour plots of the solution at* $t = 0.05$ *(left) and* $t = 30$ *(right).*

TABLE 4.2
Example 4.2: L^2*-errors with different constant time steps and a* 200×200 *grid.*

Δt	0.01	0.005	0.0025	0.00125
$\|e\|$	1.04E-2	2.90E-3	7.04E-4	1.47E-4

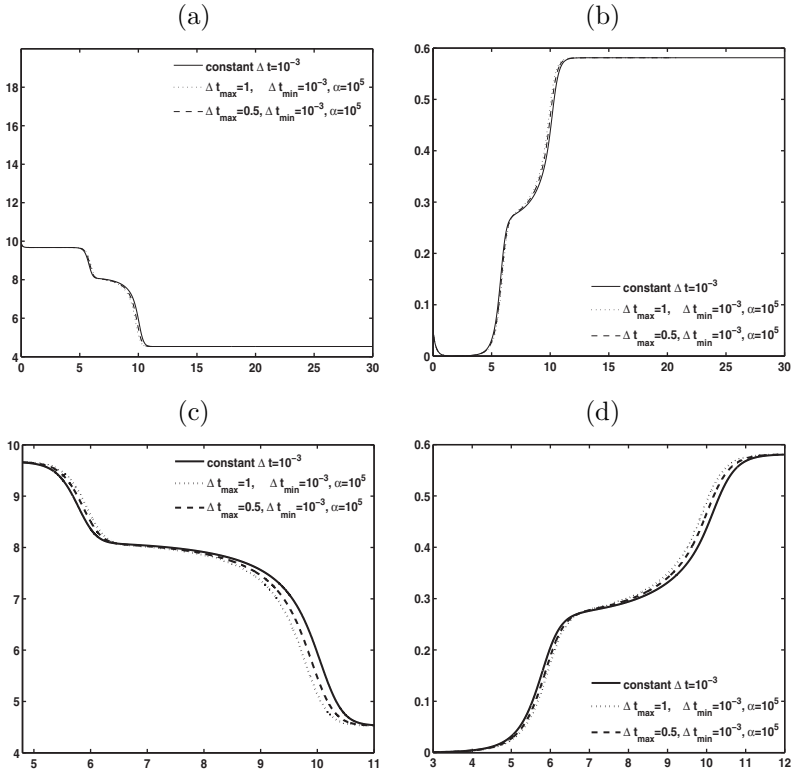

FIG. 4.5. *Example* 4.2: (a) *Evolution of energy,* $0 \le t \le 30$. (b) *Evolution of roughness,* $0 \le t \le 30$. (c) *Evolution of energy,* $4.8 \le t \le 12$. (d) *Evolution of roughness,* $3 \le t \le 13$.

In Figure 4.5, we give the roughness and energy curves obtained using constant and adaptive time steps. It is observed that with the use of adaptive time-stepping technique, the curves with $\Delta t_{\max} = 1$ and $\Delta t_{\min} = 10^{-3}$ match quite well with those

TABLE 4.3

Example 4.2: *CPU time (seconds) comparison. The adaptive time step is determined by* (3.1) *with* $\Delta t_1 = (\Delta t_{\max} = 1, \Delta t_{\min} = 0.001)$, $\Delta t_2 = (\Delta t_{\max} = 0.5, \Delta t_{\min} = 0.001)$, *and* $\alpha = 10^5$. *The constant time step* $\Delta t = 0.001$.

t	1	5	10	30	70	100	300	600
adaptive Δt_1	278	759	2287	3062	3776	4321	8013	13241
adaptive Δt_2	279	822	2393	3426	4549	5432	11925	21050
constant Δt	289	935	2496	4851	8993	12604	36783	72681

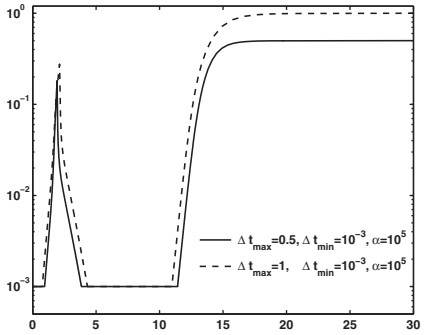

FIG. 4.6. *Example* 4.2: *The adaptive time step development with time step selection formula* (3.1).

obtained with a constant time step $\Delta t = 10^{-3}$. This implies a significant saving of CPU time.

Also we test the effectiveness of the proposed adaptive time-stepping approach. Table 4.3 lists the CPU time consumed at some selected time levels. At the early stage of the computation, both uniform time stepping ($\Delta t = 0.001$) and adaptive time stepping ($\Delta t_{\min} = 0.001, \Delta t_{\max} = 0.5$) approaches use a similar amount of CPU time because the solution has a quick transition which requires small time steps. Later, the adaptive time-stepping approach uses less and less CPU time because the solution changes slowly and as a result large time steps are allowed. During the computation, the use of time steps does not affect much on the number of the iterative steps for the Newton iteration; more precisely it takes about 1 or 2 steps for the Newton iteration. But the time steps used affect the performance of the algebraic multigrid solver. For larger time steps, the algebraic multigrid solver will take more time to solve the linear system. However, as observed in Table 4.3, the adaptive strategy can save substantial amount of the CPU time.

Also we plot the time step development in Figure 4.6. After $t = 10$, the time step approximates $\Delta t_{\max}$, so the CPU time is greatly saved as shown in Table 4.3. The parameter α plays an important role in time step selection. If α is taken too small, then it will produce large time steps during the solution transition process from $t = 3$ to $t = 10$ which is not appropriate.

Example 4.3 (coarsening dynamics). We simulate the MBE model (1.1) in two dimensions. The initial condition is a random state by a random number varying from -0.001 to 0.001 on each grid point. The domain is $\Omega = [0, 200] \times [0, 200]$ and also the problem is subject to periodic boundary conditions. We use a 400×400 grid in this simulation.

This example is aimed to apply adaptive time stepping method for studying the coarsening dynamics which has been studied extensively; see, e.g. [15, 16, 20]. Since it

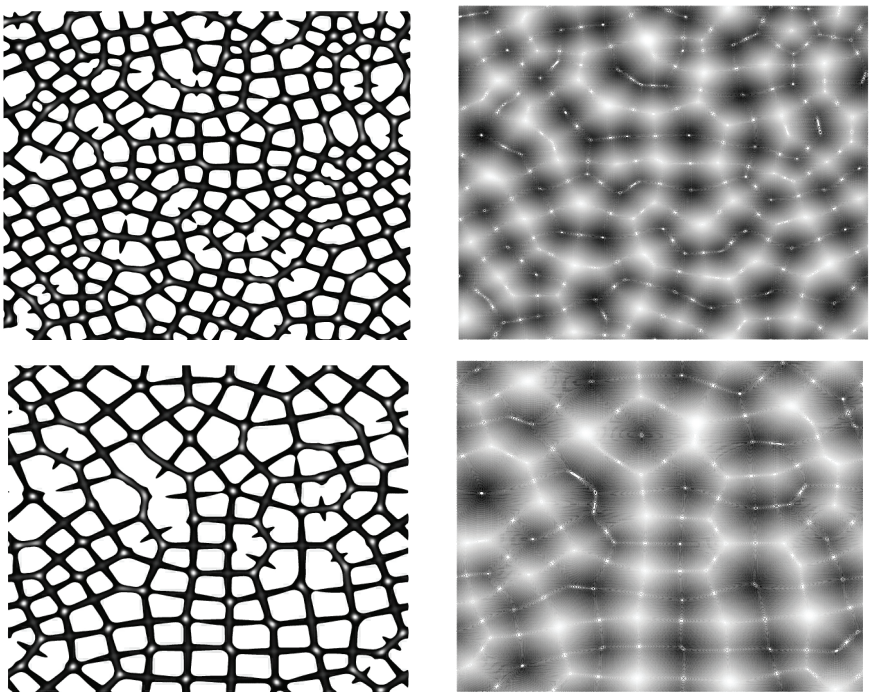

FIG. 4.7. *Example* 4.3: *The contour plot of* F_{free} *(left) and solution (right) at* $t = 2000, 5000$*, obtained by using* (3.1) *with* $\Delta t_{\max} = 10, \Delta t_{\min} = 0.5$*, and* $\alpha = 1$.

needs very long time simulations, constant time steps such as $\Delta t = 0.5$ or $\Delta t = 1$ have been used in the previous studies. In our work, we use the adaptive time step (3.1) with $\Delta t_{\min} = 0.5$, $\Delta t_{\max} = 10$ and $\alpha = 1$. The reason that we can choose smaller value of α is that in this problem the energy transition is not seen and the solution has a smooth variation. In Figure 4.7, the isolines of the free energy $F_{\text{free}}(\mathbf{x}, t)$ and the solution $\phi(\mathbf{x}, t)$ at $t = 2000$ and 5000 are plotted, respectively. The effective free energy is defined as

$$F_{\text{free}} = \frac{1}{4}(|\nabla\phi|^2 - 1)^2 + \frac{\epsilon}{2}|\Delta\phi|^2.$$

The contour lines are usually used to identify the edges of the pyramidal structures since the free energy is concentrated on the edges. The edges of the small structures of pyramids are clearly visualized in Figure 4.7. It is seen that edges of the pyramids form a random distributed network over the domain. The pyramids become large in time via a coarsening process. These observed phenomena are in a good agreement with the published results; see, e.g., [15, 20].

Figure 4.8 presents the growth of the interface height $\tilde{\phi}(t)$ and the width $\lambda(t)$ of the pyramidal structures. Here $\tilde{\phi}(t)$ is defined as

$$\tilde{\phi}(t) = \left(\frac{1}{|\Omega|}\int_\Omega \phi^2(\mathbf{x}, t)d\mathbf{x}\right)^{\frac{1}{2}}.$$

The width of the pyramid edges $\lambda(t)$ measures the mean size of the network cell, which

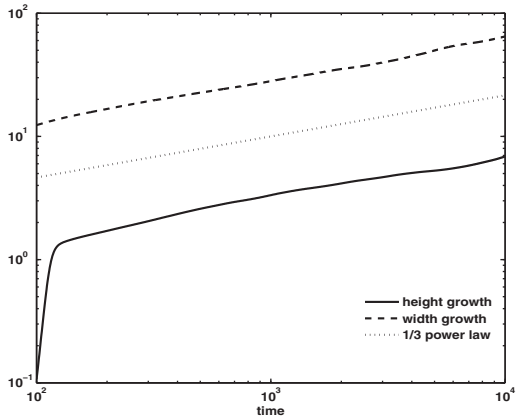

FIG. 4.8. *Example* 4.3: *Power law for height and width growth, obtained by using* (3.1) *with* $\Delta t_{\max} = 10, \Delta t_{\min} = 0.5$, *and* $\alpha = 1$.

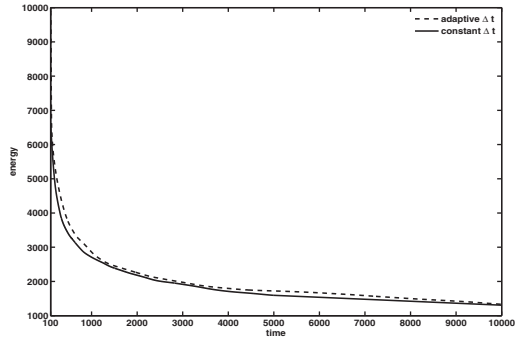

FIG. 4.9. *Example* 4.3: *Energy evolution. For adaptive time stepping,* (3.1) *is used with* $\Delta t_{\max} = 10, \Delta t_{\min} = 0.5$, *and* $\alpha = 1$. *For the constant time stepping,* $\Delta t = 0.5$.

can be calculated as suggested in [15] from the height-height correlation function

$$K_{\phi\phi}(\mathbf{r}, t) = \int_{\Omega} \phi(\mathbf{x} + \mathbf{r}, t)\phi(\mathbf{x}, t)d\mathbf{x},$$

where $\mathbf{r}$ is a positive vector. In our computation, we take a simple form $\mathbf{r} = (r, r)^T$. $K_{\phi\phi}$ can be regarded as a function of r for fixed t, which shows an oscillatory character reflecting the presence of a mound structure. For a given t, the mean pyramid width $\lambda(t)$ is defined as $r_0(t)$, which is the first zero crossing of $K_{\phi\phi}(\mathbf{r}, t)$,

$$r_0(t) = \inf \{r > 0, K_{\phi\phi}(\mathbf{r}, t) = 0\}.$$

Figure 4.8 shows the growth of the height and width against the time. After the early stage of the rearrangement of the structure, height and width satisfy the power law ct^{γ} with $\gamma = \frac{1}{3}$.

The energy evolution is plotted in Figure 4.9. The energy curve using constant time step $\Delta t = 0.5$ is also plotted in the same figure. Both curves are found well matched. The initial random state quickly develops into ordered structures and then coarsening dynamics become dominated. The energy decays quickly at the early stage and then decays slowly. Corresponding to the energy evolution, the time step increases

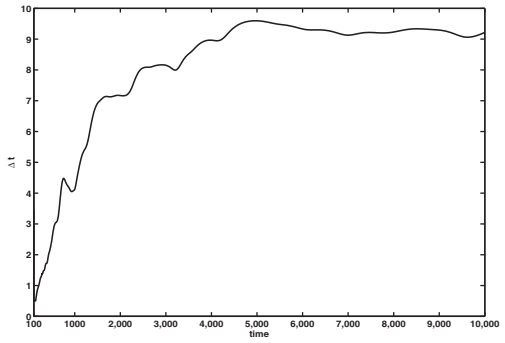

FIG. 4.10. *Example* 4.3: *Adaptive time step evolution. Equation* (3.1) *is used with* $\Delta t_{\max} = 10, \Delta t_{\min} = 0.5$, *and* $\alpha = 1$.

starting from $\Delta t = \Delta t_{\min}$ at initial time to $\Delta t \approx \Delta t_{\max}$ at about $t = 4000$. From then on, the time step is always taken close to $\Delta t_{\max}$ due to the slow variation of the energy. In Figure 4.10, it is noted that unlike previous examples, the energy does not have structure transition (i.e., the energy curve decays smoothly and monotonously). Consequently, the time step curve does not have a large variation in any short time ranges; see, e.g., Figure 4.10.

5. Concluding remarks. In this work, we have developed and analyzed two unconditionally energy stable numerical schemes for a class of nonlinear diffusion equations modeling epitaxial growth of thin films. One scheme deals with the diffusion term explicitly using the extrapolation of the known data, the other scheme approximates the diffusion terms implicitly using the average of the known and unknown levels. If large time stepping is used, the long time simulation converges to the correct steady-state solution due to the unconditional stability though the dynamics of the solution may not be obtained correctly because large time step cannot capture the rapid transition of the solution.

Since our schemes are unconditionally energy stable, it is possible to combine them with some adaptive time strategy. In our variational time-stepping formula (3.1), the energy is used to monitor the change of the time steps. The idea for time adaptivity is that a large time step is used when the energy decays slowly and a small time step is used otherwise. Numerical experiments demonstrated that the adaptive time-stepping approaches can greatly save CPU time without losing accuracy. We point out that the methods developed in this work can be extended to other model problems with the long time energy decay properties.

Acknowledgments. We would like to thank Prof. Zhimin Zhang of Wayne State University, Prof. Zhizhong Sun of Southeast University, and Prof. Qin Sheng of Baylor University for helpful discussions. We would also express our deep thanks to the anonymous reviewers whose valuable comments and suggestions helped us greatly improve this paper.

REFERENCES

[1] P. AVILES AND Y. GIGA, *A mathematical problem related to the physical theory of liquid crystal configurations*, Proc. Centre Math. Anal. Austral. Nat. Univ., 12 (1987), pp. 1–16.

[2] G. S. BALL AND R. D. JAMES, *Proposed experimental tests of a theory of fine microstructure and the two-well problem*, Philos. Trans. R. Soc. Lond. A, 338 (1992), pp. 389–450.

[3] R. E. Caflisch, M. F. Gyure, B. Merriman, S. J. Osher, C. Ratsch, D. D. Vvedensky, and J. J. Zinch, *Island dynamics and the level set method for epitaxial growth*, Appl. Math. Lett., 12 (1999), pp. 13–22.
[4] S. Clarke and D. D. Vvedensky, *Origin of reflection high-energy electron-diffraction intensity oscilations during molecular-beam epitaxy: A computational modeling approach*, Phys. Rev. Lett., 58 (1987), pp. 2235–2238.
[5] Q. Du and R. A. Nicolaides, *Numerical analysis of a continuum model of phase transition*, SIAM J. Numer. Anal., 28 (1991), pp. 1310–1322.
[6] X. B. Feng and A. Prohl, *Error analysis of a mixed finite element method for the Cahn-Hilliard equation*, Numer. Math., 99 (2004), pp. 47–84.
[7] X.-B. Feng and H.-J. Wu, *A posteriori error estimates for finite element approximations of the Cahn-Hilliard equation and the Hele-Shaw flow*, J. Comput. Math., 26 (2008), pp. 767–796.
[8] G. Gioia and M. Ortiz, *Delamination of compressed thin films*, Adv. Appl. Mech., 33 (1997), pp. 119–192.
[9] Y. He, Y. Liu, and T. Tang, *On large time-stepping methods for the Cahn-Hilliard equation*, Appl. Numer. Math., 57 (2007), pp. 616–628.
[10] W. Jin and R. V. Kohn, *Singular perturbation and the energy of folds*, J. Nonlinear Sci., 10 (2000), pp. 355–390.
[11] R. Kohn and S. Müller, *Surface energy and microstructure in coherent phase transitions*, Comm. Pure Appl. Math., 47 (1994), pp. 405–435.
[12] B. Li and J.-G. Liu, *Thin film epitaxy with or without slope selection*, European J. Appl. Math., 14 (2003), pp. 713–743.
[13] R. Li, W. B. Liu, and H. P. Ma, *Moving mesh method with error-estimator-based monitor and its applications to static obstacle problem*, J. Sci. Comput., 21 (2004), pp. 31–55.
[14] S. E. Minkoff and N. M. Kridler, *A comparison of adaptive time stepping methods for coupled flow and deformation modeling*, Appl. Math. Modelling, 30 (2006), pp. 993–1009.
[15] D. Moldovan and L. Golubovic, *Interfacial coarsening dynamics in epitaxial growth with slope selection*, Phys. Rev. E, 61 (2000), pp. 6190–6214.
[16] G. Sheng, T. Wang, Q. Du, K. G. Wang, Z. K. Liu, and L. Q. Chen, *Coarsening kinetics of a two phase mixture with highly disparate diffusion mobility*, Commun. Comput. Phys., 8 (2010), pp. 249–264.
[17] G. Söderlind, *Automatic control and adaptive time-stepping*, Numer. Algorighms, 31 (2002), pp. 281–310.
[18] Z. J. Tan, Z. R. Zhang, Y. Q. Huang, and T. Tang, *Moving mesh methods with locally varying time steps*, J. Comput. Phys., 200 (2004), pp. 347–367.
[19] S. M. Wise, C. Wang, and J. S. Lowengrub, *An energy-stable and convergent finite-difference scheme for the phase field crystal equaiton*, SIAM J. Numer. Anal., 47 (2009), pp. 2269–2288.
[20] C. J. Xu and T. Tang, *Stability analysis of large time-stepping methods for epitaxial growth models*, SIAM J. Numer. Anal., 44 (2006), pp. 1759–1779.
[21] J. Zhu, L. Q. Chen, and V. Tikare, *Coarsening kinetics from a variable-mobility Cahn-Hilliard equations: Application of a semi-implicit Fourier spectral method*, Phys. Rev. E, 60 (1999), pp. 3564–3572.